symmetry

MDPI

Article

mmWave Polarization Diversity Wideband Multiple-Input/Multiple-Output Antenna System with Symmetrical Geometry for Future Compact Devices

Mehr E Munir [1,2], Saad Hassan Kiani [3,*], Huseyin Serif Savci [3], Daniyal Ali Sehrai [4,*], Fazal Muhammad [5], Ayyaz Ali [6], Hala Mostafa [7] and Naser Ojaroudi Parchin [8]

1 Smart Systems Engineering Laboratory, College of Engineering, Prince Sultan University, Riyadh 11586, Saudi Arabia; mmunir@psu.edu.sa
2 Electrical Engineering Department , Iqra National University, Peshawar 25000, Pakistan
3 Electrical and Electronics Engineering Department, Faculty of Engineering and Natural Sciences, Istanbul Medipol University, Istanbul 34810, Turkey; hsavci@medipol.edu.tr
4 Institute for Systems and Computer Engineering, Technology and Science (INESC TEC), 4200-465 Porto, Portugal
5 Department of Electrical Engineering, University of Engineering and Technology, Mardan 23200, Pakistan; fazal.muhammad@uetmardan.edu.pk
6 Department of Electrical Engineering, National University of Sciences and Technology, Islamabad 44000, Pakistan; ayaz.phd@students.mcs.edu.pk
7 Department of Information Technology, College of Computer and Information Sciences, Princess Nourah bint Abdulrahman University, Riyadh 11671, Saudi Arabia; hfmostafa@pnu.edu.sa
8 School of Computing, Engineering and the Built Environment, Edinburgh Napier University, Edinburgh EH10 5DT, UK; n.ojaroudiparchin@napier.ac.uk
* Correspondence: iam.kiani91@gmail.com (S.H.K.); danyalkhan134@gmail.com (D.A.S.)

Abstract: The fifth generation (5G) of mobile networks is a significant technological advancement in telecommunications that provides faster data speeds, lower latency, and greater network capacity. One of the key technologies that enables 5G is multiple-input/multiple-output (MIMO) antenna systems, which allow for the transmission and reception of multiple data streams simultaneously, improving network performance and efficiency. MIMO is essential to meeting the demand for higher data rates and improved network performance in 5G networks. This work presents a four-element MIMO antenna system dedicated to the upper 5G millimeter-wave (mmWave) spectrum. The suggested antenna system is designed using an ultra-thin RO5880 substrate having total dimensions of 20 × 20 × 0.254 mm^3 with symmetrical geometry. The proposed antenna covers a fractional bandwidth of 46.875% (25–38 GHz), covering potential 5G bands of 26, 28, and 32 GHz, and offers isolation of >18 dB. The proposed MIMO system is fabricated and tested in-house. The antenna showed efficiency >88% at the potential band of interest and a peak gain of 3.5 dBi. The orthogonal arrangement of the resonating elements provides polarization diversity. Also, the MIMO parameters obtained, such as mean effective gain (MEG), envelope correlation coefficient (ECC), diversity gain (DG), channel capacity loss (CCL), and total active reflection coefficient (TARC), are found to have good performance. The measured results obtained are found to be in good agreement with simulations, hence making the proposed MIMO antenna suitable for handheld mmWave 5G devices.

Keywords: 5G; MIMO; mmWave; polarization diversity

Citation: Munir, M.E.; Kiani, S.H.; Savci, H.S.; Sehrai, D.A.; Muhammad, F.; Ali, A.; Mostafa, H.; Parchin, N.O. mmWave Polarization Diversity Wideband Multiple-Input/Multiple-Output Antenna System with Symmetrical Geometry for Future Compact Devices. *Symmetry* **2023**, *15*, 1641. https://doi.org/10.3390/sym15091641

Academic Editors: Muharrem Karaaslan and Sergei D. Odintsov

Received: 25 July 2023
Revised: 11 August 2023
Accepted: 22 August 2023
Published: 25 August 2023

1. Introduction

The millimeter-wave (mmWave) spectrum is an important part of the fifth-generation (5G) technology. mmWave refers to radio frequencies between 30 and 300 GHz, which are much higher than the frequencies traditionally used for mobile communications. In contrast, fourth-generation 4G networks typically use frequencies below 6 GHz. mmWave spectrum offers several advantages for 5G networks, including high data rates crucial for many 5G

applications such as fixed wireless access (FWA), virtual reality (VR), smart cities, the internet of things (IoT), and vehicle-to-everything (V2X) communication [1–3]. Also, mmWave advantages include low latency and larger bandwidths than traditional mobile frequencies, which allows more data to be transmitted over the network. Multiple-input/multiple-output (MIMO) antennas are essential for 5G communication in the mmWave spectrum because they can help overcome the challenges posed by the high-frequency bands [4–6]. MIMO technology employs multiple antennas at both the transmitting and receiving ends to transmit and receive data simultaneously, increasing spectral efficiency and reducing interference. In the mmWave spectrum, MIMO antennas can help improve signal quality, increase data rates, and extend the range of 5G networks. With MIMO, beamforming can be used to direct the signal toward the intended receiver and mitigate interference from other sources, improving the overall network performance. Since mmWave signals can be easily obstructed by obstacles, MIMO antennas can help overcome these obstructions and maintain a stable and strong connection between the device and the network [7,8]. The use of MIMO antennas in the mmWave spectrum is critical for enabling the high data rates and low latency that 5G promises, making it an essential technology for the future of mobile communication.

Various MIMO antenna designs have been suggested in the existing literature [9–15]. In [9], a design has been developed for a dual-band, dual-linear-polarization reflectarray aimed at future 5G cellular applications. This design incorporates a single-layer unit cell consisting of two sets of miniature fractal patches. The unit cell enables dual-polarization operation at distinct frequencies within the Ka-band (27/32 GHz). Extensive analysis confirms the independent behavior of the unit cell across the desired frequency bands and polarizations. The proposed architecture boasts small unit cell sizes, minimal losses, a thin and simple construction, and the ability to optimize phase independently for each frequency and polarization. The dual-band, dual-polarized reflectarray cell is formed by combining two sets of miniature patches printed on a single substrate layer. Each set operates at a specific resonant frequency and provides two linearly polarized elements, each rotated by 90 degrees, thereby facilitating a dual-polarization operation mode. In [10], a comparison was made between four different types of random arrays by calculating their array factor's mean and variance. This enabled a partial statistical characterization of these arrays and established a link between the elemental count and aperture of the array with specific key characteristics. Since there was no straightforward analytical tool that could accurately measure the side-lobe level, the experimental aspect was given additional importance. For the purpose of achieving results and in order to experimentally analyze the side-lobe distribution, Monte Carlo simulations were performed, considering the number of radiators and the average distance between them as variables. The results obtained from these simulations demonstrated that random arrays, which allowed for restrictions on the minimum distance between adjacent components, achieved comparable performance to other methods without such limitations. Random arrays were preferred due to their ability to mitigate the effects of reciprocal coupling by ensuring that neighboring radiators were not positioned closer than a predetermined minimum distance.

In [11], a four-port MIMO system is presented for central frequency of 30 GHz. The antenna showed 5 GHz bandwidth and the isolation is improved by incorporating a two-layer transmission-type frequency selective surface (FSS) superstrate based on planar crossed-dipole metal. After the insertion of FSS, the isolation up to 6 dB and gain up to 5 dB is improved. In [12], a novel MIMO antenna system is presented that draws inspiration from the natural world. The central frequency of the proposed antenna system is 28 GHz, which is suitable for future millimeter-wave technologies. The antenna system contains four resonators arranged in a compact configuration, which enables it to achieve high gain and directivity. The authors used a fractal geometry inspired by the Mandelbrot set to design the individual antenna elements. This geometry provides multiband operation and enhances the bandwidth of the antenna system. The proposed MIMO antenna system also has high isolation of 25 dB between the elements.

In [13], a mmwave antenna system with 4G antennas are presented together at chassis with dimensions of 150 × 77.8 mm^2. The isolation among mmwave elements is noted to be nearly 20 dB and ECC < 0.0125. To enhance the separation between the 5G and 4G signal sources, a low-pass filter (LPF) is included. This LPF is created using a stepped impedance approach, which involves using sections of transmission lines with extremely high and very low characteristic impedance. A shared-aperture beam-scanning antenna array that operates in both Ku and Ka frequency bands is presented in [14]. The implemented antenna design utilizes four linear antenna arrays operating in the Ku-band and four linear antenna arrays operating in the Ka-band. These arrays are constructed using substrate-integrated waveguide (SIW) technology. By using the Ku-band antenna as the side walls of the Ka-band antenna, the element spacing at both frequency bands is optimized for wide-scan operation. SIW power dividers and printed circuit board (PCB) fabrication techniques are employed to design the feeding networks for the two arrays. The design also incorporates self-filtering, orthogonal polarization and optimal array layout to ensure a high level of channel isolation between the two antennas operating at different frequency bands throughout the entire range of beam scanning. Experimental validation confirms that the achieved isolation between the antennas surpasses 28 dB at Ku-band and 70 dB at Ka-band, even under scanning angles of up to 40 degrees. This excellent isolation performance highlights the effectiveness of the proposed shared-aperture concept and the validity of the design results. One of the advantages of this design is its compact topology, but a potential limitation is the complexity of fabrication due to the use of SIW technology.

The antenna presented in [15] is designed as a monopole antenna. It consists of a circular patch with a rectangular slot cut out from it, along with a partial ground plane. This specific antenna is intended to work within a frequency range spanning from 36.6 GHz to 39.5 GHz, with the center frequency being 38 GHz. To enhance the antenna's performance, measures have been taken to minimize interference between different parts of the antenna setup. Four stubs have been added strategically to reduce unwanted interaction between antenna elements at the desired frequency bands. This is crucial to achieve a high level of isolation, ensuring that the signals transmitted and received by the antenna remain clear and distinct. Moreover, in order to boost the antenna's signal strength, an FSS sheet is incorporated. This FSS is designed to function at the same frequency bands as the antenna and is positioned underneath the suggested MIMO system. This FSS acts like a reflector, directing and focusing the signals in a specific direction, thereby increasing the antenna's gain or signal strength. However, one primary drawback is the antenna's relatively narrow bandwidth. It can only effectively operate within a small range of frequencies from 36.6 GHz to 39.5 GHz. Another challenge arises from the integration of the frequency-selective structure at millimeter-wave frequencies. Millimeter-wave technology operates in extremely high-frequency ranges, which can make the fabrication and implementation of these structures quite complex, especially in compact devices.

Similarly, in [16], a four-element MIMO system is presented with bandwidth ranging from 27 to 29 GHz. By employing the spatial diversity approach, the isolation of the antenna system has been significantly enhanced, achieving isolation levels of more than 24 dB across the desired frequency range. Several isolation techniques help in minimizing the coupling among radiating elements. These techniques include the use of electromagnetic bandgap structures (EBG) [17,18], defected ground structures (DGS) [19,20], and meandered line resonators [21,22]. In [17], with the use of EBG and hairpin shape DGS, the isolation among radiating elements was improved up to 32 dB.

This article presents a four-element printed MIMO antenna operating over mmwave spectrum from 25 to 38 GHz. The proposed MIMO systems offer polarization diversity characteristics with self-isolation of >24 dB throughout the band of interest. The antenna is fabricated and tested using an in-house facility. The other MIMO parameters are tested and found to be in safe limits. The structure of the paper is as follows.

The literature review and detailed introduction is given in Section 1. Section 2 covers the working principle of antenna and MIMO configuration. Section 3 shows the fabricated

prototype and obtained results discussion, followed by a comparison table with the state-of-the-art technology and a conclusion.

2. Antenna Design

The proposed antenna is shown in Figure 1. The plow-shaped antenna comprises of a four resonating strips with two strips turned at certain angle. These strips generate the wideband response. The proposed antenna is designed on ultra-thin 0.254 mm R05880. The ground plane consists of a tunable notch at the top mid-section of ground plane. The designed is simulated in Computer Simulation Technology (CST) 2019 with higher meshing environment of 15 cells per wavelength. The complete dimensions of the proposed antenna in millimeters (mm) is shown in Table 1.

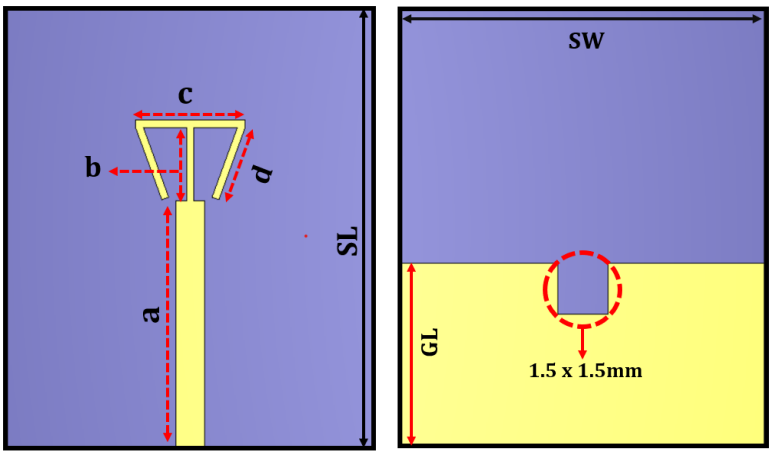

(**a**) (**b**)

Figure 1. Proposed plow-shaped antenna (**a**) front and (**b**) back.

Table 1. Proposed Antenna Dimensions.

Parameter	a	b	c	d	SL	SW	GL	Angle
Value (mm)	6.75	2.5	2.75	2.45	10	12	5	20

Figure 2 explains the design evolution process of the proposed antenna. The effective length of the resonating element with the contribution of each segment has been derived using the following equation. It is shown.

$$L_{eff} = c + 2 * d * cos(ang) * m1 - 2 * d * sin(ang) * m2 \quad (1)$$

where c is the length of the horizontal segment, d is length of the tilted vertical segments at each end of the segment c. ang is the angle between c and d, which is 20°. The segment d has vertical and horizontal components which have lengths defined by $d * sin(20)$ and $d * cos(20)$, respectively. The currents flowing through the segments $d * sin(20)$ and $d * cos(20)$ would generate some opposing currents flowing on the segments c and b due to the mutual coupling. Therefore these opposing currents would cause some degree of cancellation in the corresponding segments. This effect manifests itself as some reduction in the length. The degree of reduction is given with the parameters $m1$ and $m2$ in the equation. $m1$ defines the percentage of length on each vertical segment of d that is left after the coupling effect due to the currents of b. Similarly $m2$ defines the percentage of length on each horizontal segment of d that will be subtracted from c. The L_{eff} causes the resonance on the unit cell response. The frequency of this resonance is given by the following equation.

$$L_{eff} = \frac{C}{2f_0\sqrt{\epsilon_{reff}}} \quad (2)$$

where C is the speed of light, f_0 is the operating frequency and ϵ_{reff} is the effective dielectric constant.

$$\epsilon_{reff} = \frac{\epsilon_r + 1}{2} \tag{3}$$

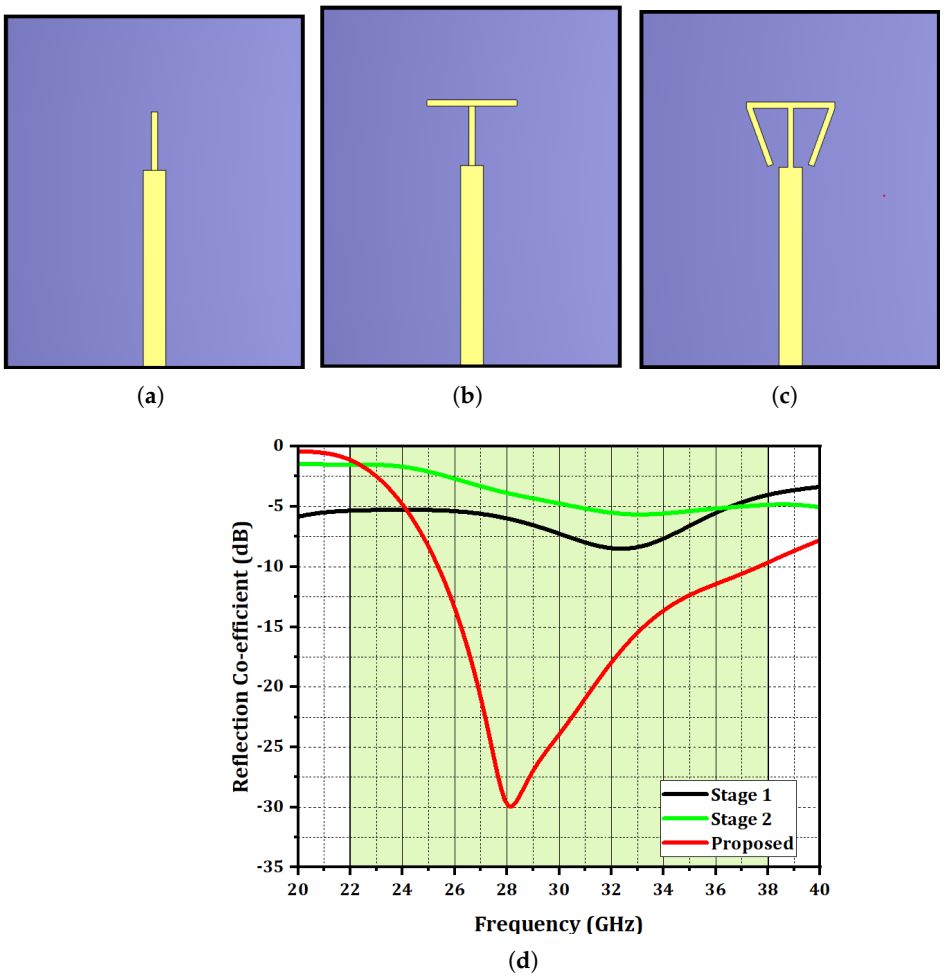

Figure 2. Design evolution. (**a**) Stage 1. (**b**) Stage 2. (**c**) Proposed. (**d**) Reflection co-efficient.

Figure 3 shows the parametric analysis of the proposed plow-shaped antenna. The two parameters analyzed are the ground notch and the angle among the plow-shaped strips. Both parameters play a significant role in shifting the antenna frequency. Figure 3a shows the resonance response with respect to incident angle among strips while Figure 3b shows the response with respect to ground notch. As seen from the Figure, the angle between the strips of plow-shaped antenna plays a significant role in resonance. As the angle is decreased, the resonance frequency is diminished. The desired resonance response occurs at an angle of 20°. At a 25° angle, the resonance moves to the higher frequency of 31 GHz. Similarly, the ground notch helps in matching the impedance of the antenna on the desired frequency. With a value of 1.4 mm, the ground notch exhibits resonance from 25 to almost 39 GHz but with the maximum return loss value of 18 dB. The desired response is achieved at 1.5 mm where the return loss value of 30 dB is achieved but with the trade-off on bandwidth. The bandwidth at the higher value is decreased from 39 to 38 GHz. Further increase in ground slot value shifts the frequency to a higher value and also decreases the bandwidth response.

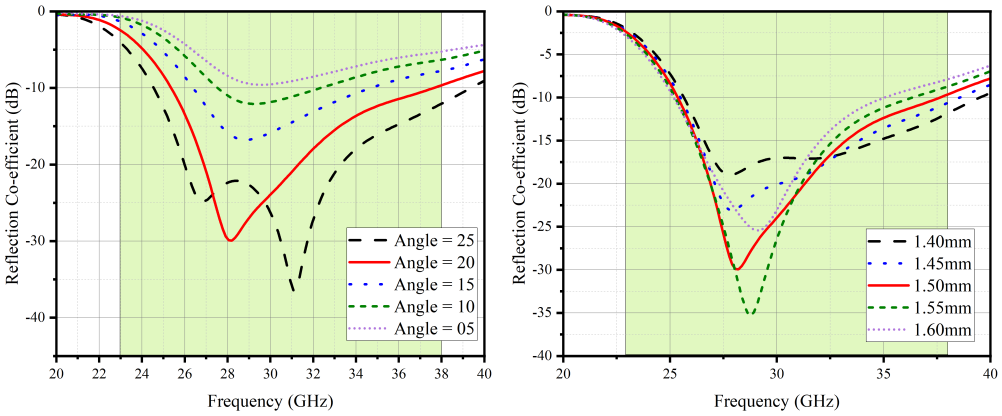

Figure 3. Parametric analysis. (**a**) Angle. (**b**) Ground notch with respect to width.

Figure 4 presents the surface current distribution and the gain with the efficiency of the antenna. The surface current presented at 28 GHz resonance shows the significance of the angled strips and notch in generating the desired wideband response. The efficiency ranges between 94 and 96% for radiation efficiency, while for total efficiency, it is between 80 and 92%. The gain at 28 GHz is noted to be 3.2 dBi.

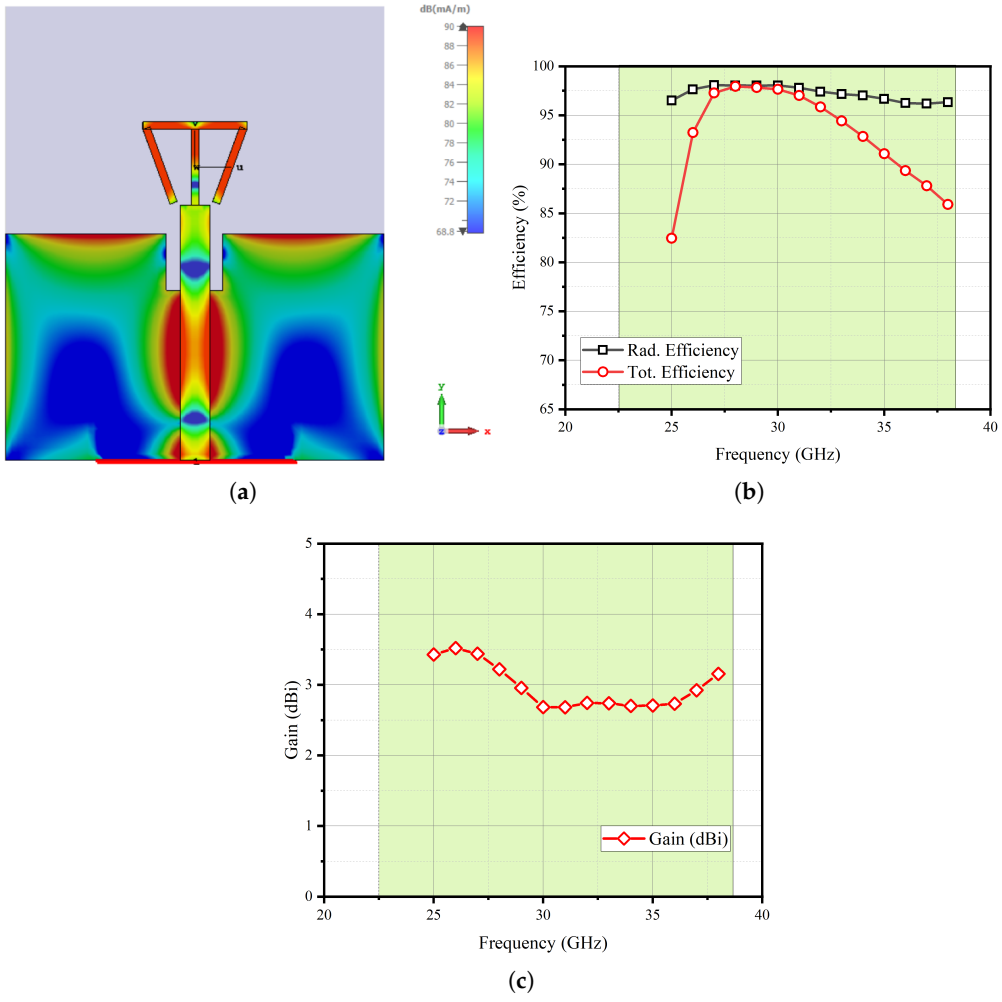

Figure 4. (**a**) Surface currents. (**b**) Simulated efficiencies. (**c**) Gain.

3. Results and Discussions

3.1. MIMO Configuration

The plow-shaped antenna design presented in this study has been adapted into a MIMO system consisting of four elements. MIMO antennas offer increased data throughput, enhanced spectral efficiency, improved link reliability, extended range and coverage, and support for multiple users, resulting in faster and more reliable wireless communication, efficient spectrum utilization, and improved network performance in challenging environments. Figure 5 shows the proposed MIMO system front and back view. The MIMO antennas are arranged in such a way that each neighboring antenna is set to be at 90°. The scattering parameters, known as S-parameters, were simulated and measured for each MIMO configuration implemented as an integrated design. This was performed to analyze and document the practical and simulated characteristics of the design. The Anritsu Shock Line MS46122B Vector Network Analyzer (VNA) was employed to measure the S-parameters. The reflection coefficient response for all MIMO elements is identical as compared to the measured response as shown in Figure 6.

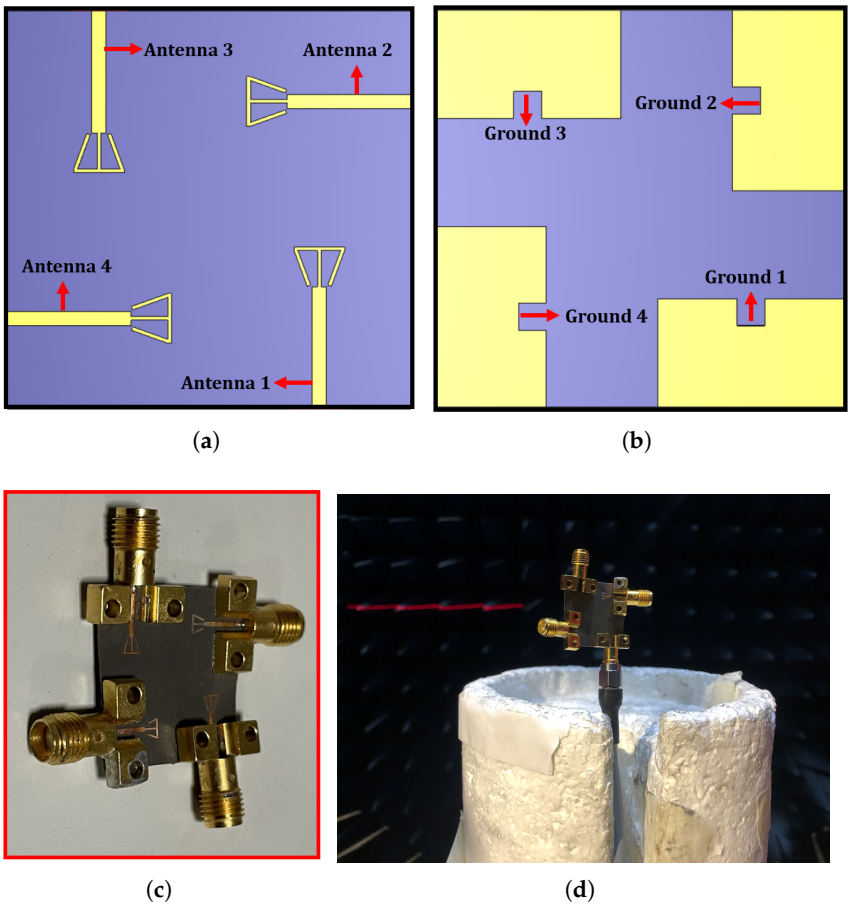

Figure 5. MIMO antenna configuration. (**a**) Front. (**b**) Back. (**c**) Fabricated prototype. (**d**) Far-field measurement setup.

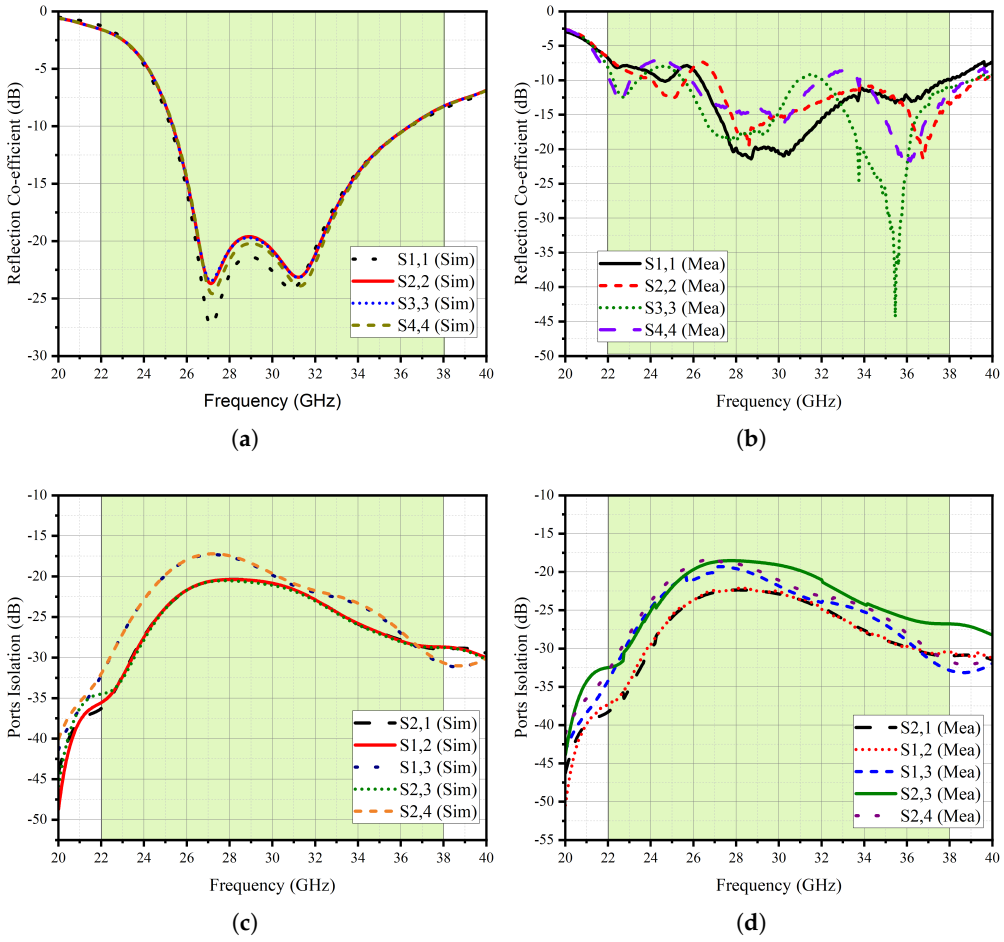

Figure 6. (**a**) Reflection co-efficient simulated. (**b**) Reflection co-efficient measured. (**c**) Port isolation simulated. (**d**) Port isolation measured.

Slight disruptions have been noted which can be attributed to measurement and environmental errors. Notably, a noteworthy achievement is minimum isolation of >18 dB, indicating remarkably strong practical isolation characteristics. The measured results also reveal that the antenna's effective bandwidth in real-world scenarios matches the simulated bandwidth claimed, confirming consistency between theory and practical implementation. The simulated and measured total efficiencies and gain are given in Figure 7. The efficiencies range between 80 and 96%, while for 28 GHz, it is noted to be 92%. The peak gain recorded is 6.2 dBi at 28 GHz.

3.2. Radiation Patterns

One important aspect of MIMO antenna systems is the radiation pattern and pattern diversity. The radiation pattern refers to the spatial distribution of electromagnetic energy radiated by an antenna. In MIMO systems, each antenna element has its own radiation pattern, and the combined patterns of all the antennas contribute to the overall system performance. Pattern diversity is the ability of MIMO antennas to provide multiple spatial paths for signal propagation, which helps mitigate the effects of multipath fading and improves system reliability. By exploiting the diverse radiation patterns, MIMO systems can achieve spatial multiplexing, where multiple data streams can be transmitted simultaneously in different spatial directions, leading to increased data rates and improved system capacity. Moreover, pattern diversity allows for better signal coverage, spatial selectivity, and interference rejection, making MIMO antenna systems a valuable technology for modern wireless communication applications. Figure 8 shows the radiation pattern of the

MIMO system. The patterns presented are at the resonance frequency of 28 GHz at yx and zx plane.

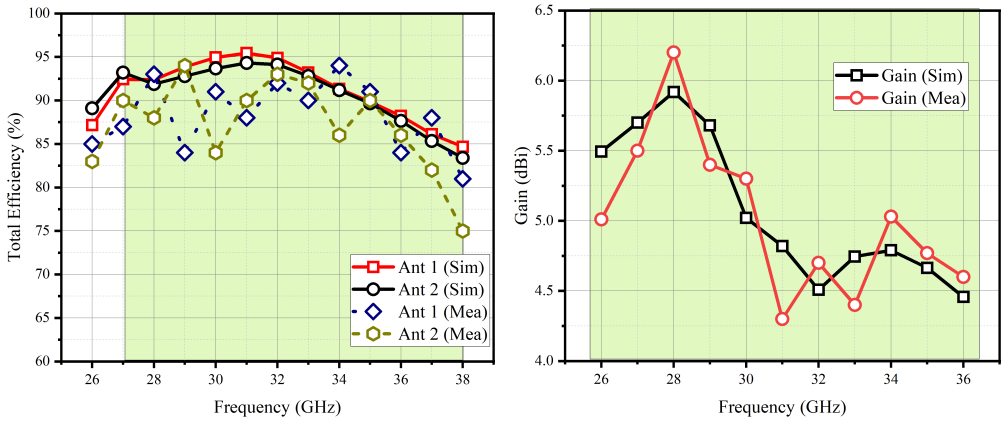

Figure 7. Simulated and measured (**a**) total efficiency and (**b**) gain.

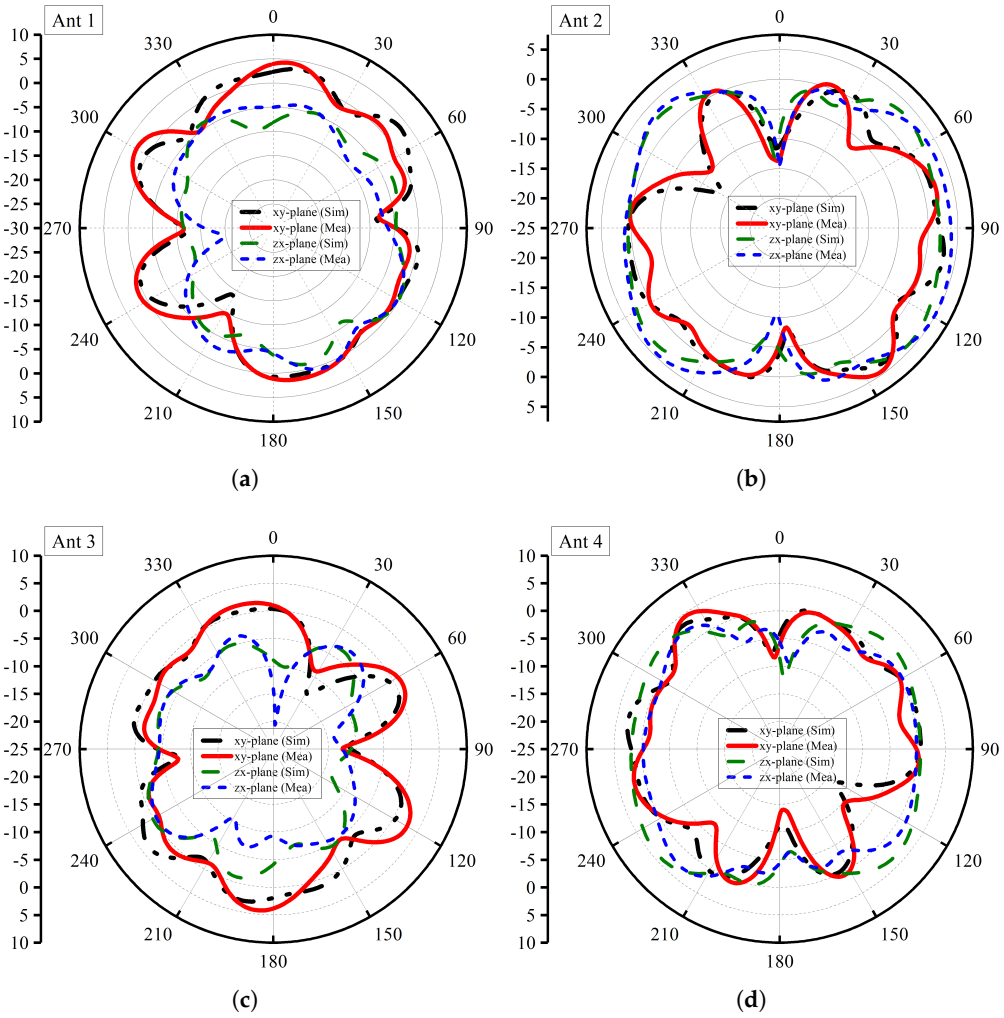

Figure 8. Simulated and measured radiation at xy and zx planes. (**a**) Ant1; (**b**) Ant2; (**c**); Ant3; (**d**) Ant4.

As seen from the figure, the proposed antenna exhibits polarization diversity characteristics as at the *xy*-plane; the Ant1 main lobe is at 52°, while for Ant 2, it is at 141°. Similarly, for Ant 3, the direction of radiation is between 210° and 240°, while for Ant 4 it is at 322°. This diversity characteristic has also been observed at the *zx*-plane for the proposed MIMO system. The co- and x-polarization are shown in Figure 9. From the figure, the x-pol levels of the MIMO system are well below −11 dB.

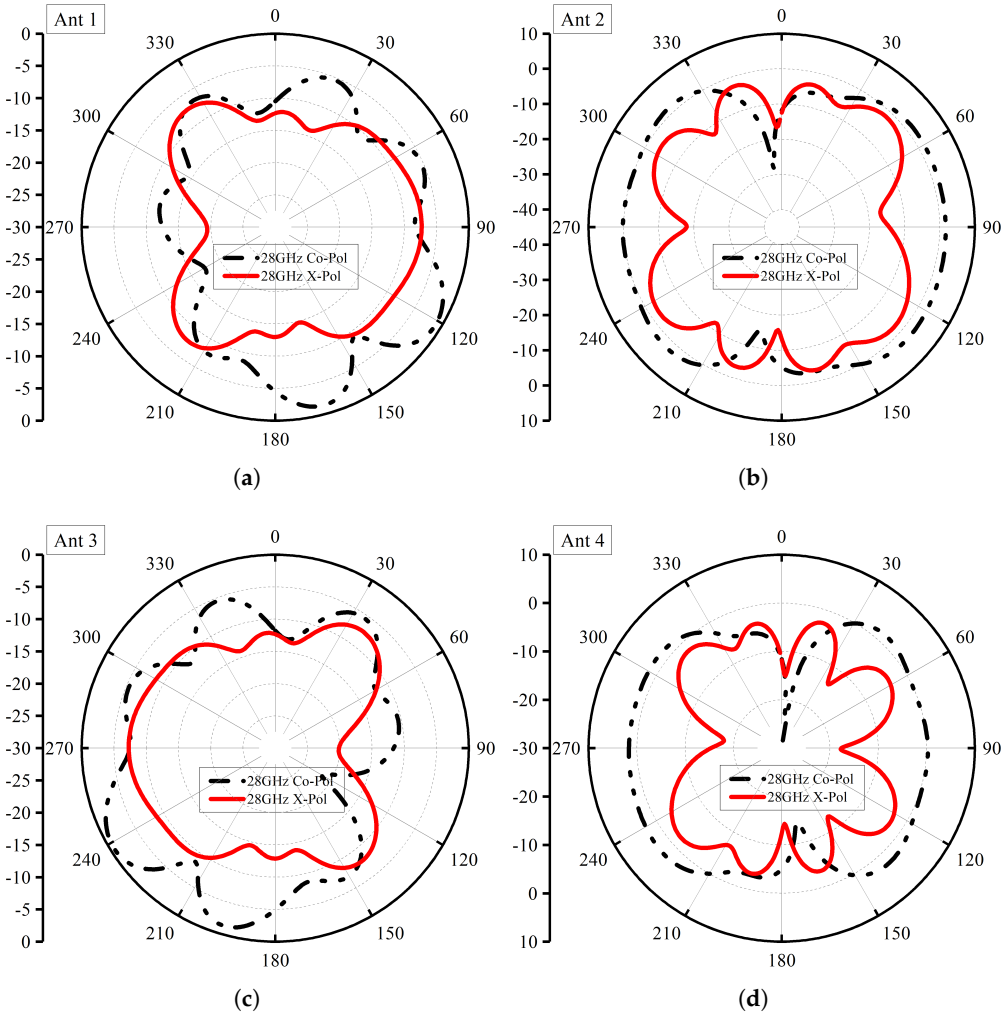

Figure 9. Co- and x-pol at 28 GHz. (**a**) Ant1; (**b**) Ant2; (**c**) Ant3; (**d**) Ant4.

4. MIMO Performance Parameters

MIMO performance parameters are metrics used to evaluate the effectiveness and efficiency of MIMO antenna systems in wireless communication. These parameters provide insights into the system's capacity to improve data rates, enhance signal quality, mitigate interference, and achieve reliable transmission in multi-path environments. These parameters include the envelope correlation coefficient (ECC), mean effective gain (MEG), and diversity gain (DG). ECC is an important parameter in MIMO systems that quantifies the correlation between the signals received by different antenna elements. It reflects the degree of spatial correlation and mutual coupling between the antennas. The ECC of the proposed plow-shaped MIMO antenna system is derived using far-field characteristics as given in Equation (1) [23,24]. The ECC among any two radiating elements is found to be less than 0.2, as shown in Figure 10a,b. Similarly, relying solely on stand-alone antenna gain as a measure of performance can be unreliable, as antennas are commonly used in real-world settings rather than in anechoic chambers. The criteria for the proposed system are as follows. Antennas operate in specific situations and for specific applications,

and it is crucial to consider the impact of the surrounding environment on their radiation properties in order to accurately assess their performance. The mean effective gain (MEG) offers valuable insights into the anticipated performance of the antenna in a multi-path environment, providing an understanding of its ability to handle signal reflections and interference caused by multipath propagation by considering the complex interactions and reflections that occur in real-world scenarios. The MEG of the investigated MIMO system is shown in Table 2. The MEG is calculated using Equation (2) mentioned in [25,26]. Diversity gain is the measure of signal quality improvement obtained by utilizing multiple antennas in a MIMO system. In MIMO systems, the normal range for diversity gain typically falls between 9.95 to 10 dB. Figure 8c shows the DG of the MIMO system. The evaluation of performance parameters revealed that all results were within acceptable limits, confirming that the antenna system satisfies the desired performance requirements.

$$ECC = \frac{|\iint_{4\pi}(\vec{B}_i(\theta,\phi)) \times (\vec{B}_j(\theta,\phi))\, d\Omega|^2}{\iint_{4\pi}|(\vec{B}_i(\theta,\phi))|^2\, d\Omega \iint_{4\pi}|(\vec{B}_j(\theta,\phi))|^2\, d\Omega} \tag{4}$$

where $\vec{B}_i(\theta,\phi)$ denotes the 3D radiation pattern upon excitation of the i antenna and $\vec{B}_j(\theta,\phi)$ denotes the 3D radiation pattern upon excitation of the jth antenna. Ω is the solid angle.

$$MEG = \int_{-\pi}^{\pi}\int_{0}^{\pi}[\frac{r}{r+1}G_\theta(\theta,\phi)P_\theta(\theta,\phi) + \frac{1}{1+r}G_\phi(\theta,\phi)P_\phi(\theta,\phi)]sin\theta d\theta d\phi \tag{5}$$

where $G_\phi(\theta,\phi)$ and $P_\theta(\theta,\phi)$ are angle of arrival and r is the cross-polar ratio, which can be expressed as Equation (6).

$$r = 10log_{10}(\frac{P_{vpa}}{P_{hpa}}) \tag{6}$$

The power received by the vertically polarized and horizontally polarized antenna is represented as P_{vpa} and P_{hpa}, respectively.

$$DG = 10\sqrt{1-(ECC^2)} \tag{7}$$

In MIMO antenna systems, TARC is a crucial parameter that measures the efficiency of the antenna system in transmitting and receiving signals with minimal reflection losses [25,26]. A low TARC value indicates that the MIMO system can effectively transfer signals without significant losses due to reflection. This leads to improved signal quality, higher data rates, and increased overall system capacity, which are essential for achieving reliable and high-performance wireless communication. For calculating the TARC, the laboratory-measured S-parameters of a two-element MIMO antenna were used. From Figure 10d, the TARC can be seen below 10 dB for the whole band of interest.

Channel capacity loss in MIMO antenna systems refers to the reduction in the maximum data rate due to practical constraints of the wireless channel. Multiple factors contribute to this phenomenon, including spatial correlation between antennas, fading, interference from other networks, and the presence of noise [27,28]. In an ideal scenario, the desired value for channel capacity loss in MIMO antenna systems would be zero, indicating no loss or degradation in the maximum achievable data rate [29]. However, achieving zero channel capacity loss is practically unattainable due to the inherent limitations and constraints of the wireless environment [30]. From Figure 10e, channel capacity loss is observed below 0.5 bits/s/Hz in the operating frequency bands, which satisfies its acceptable limit condition.

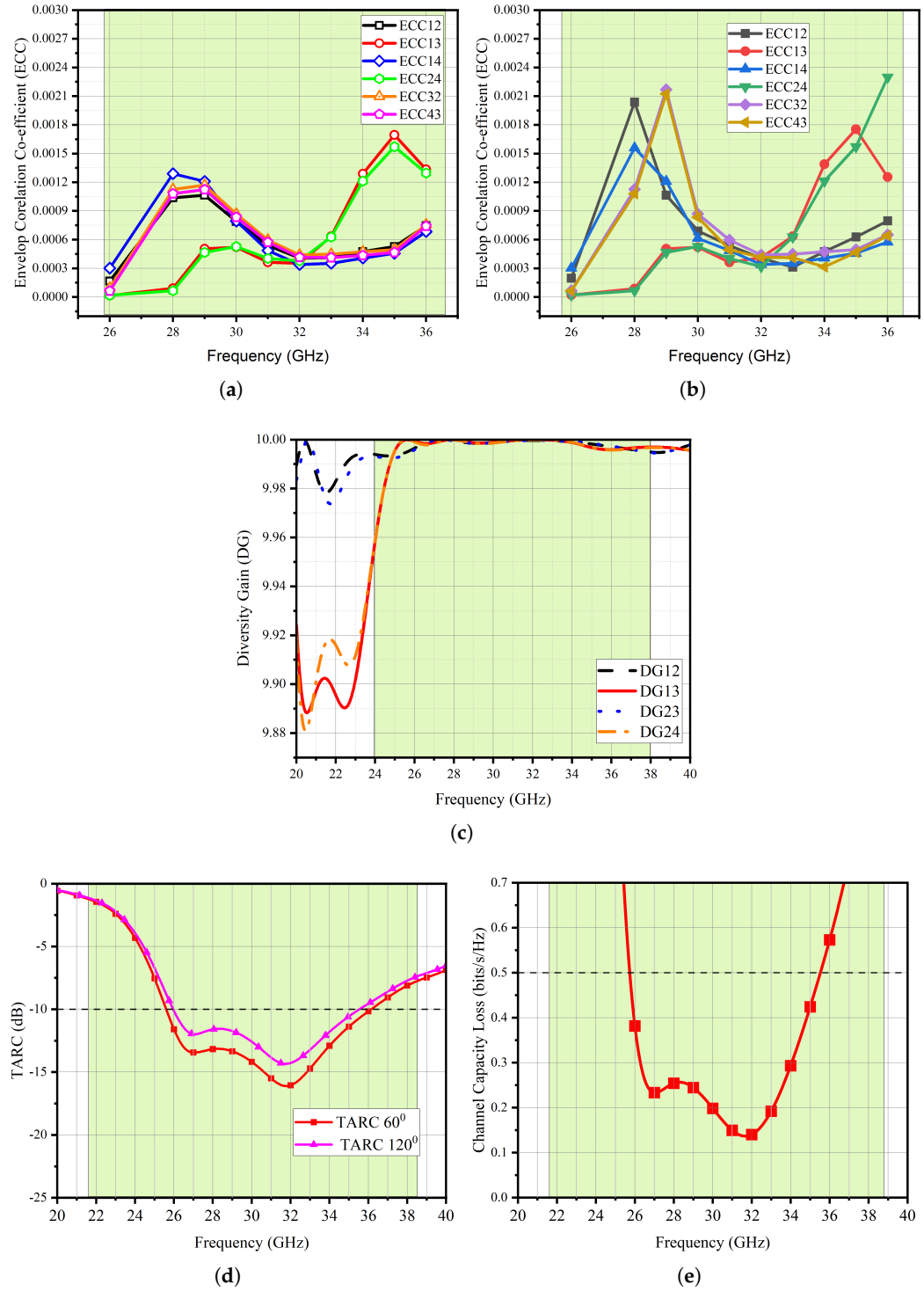

Figure 10. Olympeak antenna MIMO parameters. (**a**) ECC Sim. (**b**) ECC Mea. (**c**) Diversity gain. (**d**) TARC. (**e**) CCL.

Table 3 presents a comparison between the proposed work and the existing literature, shedding light on the advantages offered by the novel antenna design. Among the standout features, the most striking is its compact size, a testament to the ingenuity and innovation behind this research. By achieving a smaller form factor, the proposed antenna opens up exciting possibilities for integration into various compact devices and space-constrained applications without compromising on performance. Equally impressive is

the wide bandwidth response showcased by the proposed antenna, surpassing what has been previously reported in the published literature. This expanded bandwidth translates into faster data transmission, reduced latency, and enhanced overall communication efficiency, a crucial factor in today's fast-paced digital landscape. As data-hungry applications and emerging technologies continue to thrive, the ability of the proposed antenna to accommodate such demanding data rates is nothing short of a game-changer. Moreover, the exceptional isolation and ECC (envelope correlation coefficient) levels exhibited by the antenna further underscore its excellence in design and engineering. Isolation is a pivotal aspect in multiple-antenna systems as it determines the ability to minimize interference and cross-talk between antennas. With superior isolation, the proposed antenna ensures cleaner signal reception, reduced signal degradation, and heightened system reliability, all of which contribute to an unparalleled user experience. The high ECC levels are equally noteworthy as they signify the antenna's ability to maintain consistent performance across its multiple input channels. This translates to improved stability, reduced signal distortion, and enhanced signal diversity, which is especially critical in achieving seamless connectivity and data transmission in MIMO configurations. In summary, the proposed work represents a substantial leap forward in antenna design, offering an enticing combination of compactness, wide bandwidth response, excellent isolation, and remarkable ECC levels. Its potential applications span a broad spectrum, from futuristic wireless communication systems to cutting-edge Internet of Things (IoT) devices.

Table 2. MEG of the proposed antenna system.

Frequency (GHz)	MEG1	MEG2	MEG3	MEG4
28	−3.15	−3.22	−3.65	−3.29
29	−2.99	−3.13	−3.41	−3.56

Table 3. Comparison of proposed antenna system with the literature.

Ref	Antenna Elements	Frequency (GHz)	Size (mm^2)	Isolation (dB)	ECC
[11]	4	28–33	30 × 30	<20	<0.012
[12]	4	26–30	30 × 30	<24	<0.12
[13]	4	25–40	156 × 77.8	<20	<0.0125
[15]	4	37–39	36 × 36	<25	<0.013
[20]	4	25.1–36.5	12.8 × 50	<22	<0.15
[21]	4	26–31	48 × 31	<20	<0.015
[22]	4	26.5–39.5	30 × 30	<28	<0.1
[29]	2	26.5–29.5	11 × 20	<20	<0.0115
[30]	4	25–50	33 × 33	<12	<0.005
Prop.	4	25–38	20 × 20	<18	<0.012

5. Conclusions

This study introduces a radical multiple-input/multiple-output (MIMO) antenna system designed to operate within the frequency range of 25 to 38 GHz. The antenna's planar structure is elegantly simplistic, featuring a central frequency of 28 GHz and an impressive efficiency exceeding 90% over the whole operating bandwidth. The MIMO system is a model developed and fabricated after measurement closely matched the simulated characteristics. The isolation between any two antenna elements was determined to be greater than 18 dB. Additionally, key MIMO metrics, including ECC, MEG, TARC, CCL, and DG, were all determined to fall within safe limits. Based on these exceptional outcomes, the proposed MIMO antenna system demonstrates immense potential as a leading candidate for future mmWave devices. Considering its remarkable efficiency and strong performance, this innovative antenna system holds great promise for advancing the realm of millimeter-wave technology and its applications.

Author Contributions: Conceptualization, M.E.M., F.M. and S.H.K.; methodology, H.S.S., D.A.S. and N.O.P.; software, M.E.M. and S.H.K.; validation, H.S.S. and N.O.P.; formal analysis, D.A.S. and N.O.P.; investigation, F.M. and N.O.P.; resources, A.A. and H.M.; data curation, H.S.S., D.A.S., A.A. and H.M.; writing—original draft preparation, M.E.M. and S.H.K.; writing—review and editing, S.H.K., H.S.S. and A.A.; visualization, M.E.M. and N.O.P.; supervision, M.E.M. and H.M.; project administration, A.A. and H.M.; funding acquisition, H.M. and F.M. All authors have read and agreed to the published version of the manuscript.

Funding: Princess Nourah bint Abdulrahman University Researchers Supporting Project Number (PNURSP2023R137), Princess Nourah bint Abdulrahman University, Riyadh, Saudi Arabia.

Institutional Review Board Statement: Not applicable.

Informed Consent Statement: Not applicable.

Data Availability Statement: All the data are available in the study.

Acknowledgments: The authors would like to acknowledge the support of Prince Sultan University, Riyadh, Saudi Arabia for providing funding for this article.

Conflicts of Interest: The authors declare no conflict of interest.

References

1. Kiani, S.H.; Marey, M.; Rafique, U.; Shah, S.I.H.; Bashir, M.A.; Mostafa, H.; Wong, S.-W.; Parchin, N.O. A Deployable and Cost-Effective Kirigami Antenna for Sub-6 GHz MIMO Applications. *Micromachines* **2022**, *13*, 1735. [CrossRef] [PubMed]
2. Costanzo, S.; Venneri, F.; Di Massa, G.; Borgia, A.; Costanzo, A.; Raffo, A. Fractal Reflectarray Antennas: State of Art and New Opportunities. *Int. J. Antennas Propag.* **2016**, *2016*, 7165143. [CrossRef]
3. KSaeidi, T.; Al-Gburi, A.J.A.; Karamzadeh, S. A Miniaturized Full-Ground Dual-Band MIMO Spiral Button Wearable Antenna for 5G and Sub-6 GHz Communications. *Sensors* **2023**, *23*, 1997. [CrossRef]
4. Ibrahim, M.S. Design of low-cost, circularly polarized, and wideband U-slot microstrip patch antenna with parasitic elements for WiGig and WPAN applications. *Appl. Comput. Electromagn. Soc.* **2019**, *34*, 1453–1456.
5. Sakr, A.A.; Dyab, W.M.; Wu, K. A dually polarized six-port junction based on polarization-selective coupling for polarization-inclusive remote sensing. *IEEE Trans. Microw. Theory Tech.* **2018**, *66*, 3817–3827. [CrossRef]
6. Dyab, W.; Sakr, A.A.; Wu, K. Millimeter-Wave Polarization-Inclusive Remote Sensing System Based on Dually-Polarized Six-Port Junction. In Proceedings of the 2018 11th Global Symposium on Millimeter Waves (GSMM), Boulder, CO, USA, 22–24 May 2018; IEEE: New York, NY, USA, 2018.
7. Ibrahim, M.S.; Attia, H.; Cheng, Q.; Mahmoud, A. Wideband circularly polarized aperture coupled DRA array with sequential-phase feed at X-band. *Alex. Eng. J.* **2020**, *59*, 4901–4908. [CrossRef]
8. Wani, Z.; Abegaonkar, M.P.; Koul, S.K. A 28-GHz antenna for 5G MIMO applications Progress. *Electromagn. Res. Lett.* **2018**, *78*, 73–79. [CrossRef]
9. Hussain, M.; Mousa Ali, E.; Jarchavi, S.M.R.; Zaidi, A.; Najam, A.I.; Alotaibi, A.A.; Ghoneim, S.S. Design and Characterization of Compact Broadband Antenna and Its MIMO Configuration for 28 GHz 5G Applications. *Electronics* **2022**, *11*, 523. [CrossRef]
10. Raheel, K.; Altaf, A.; Waheed, A.; Kiani, S.H.; Sehrai, D.A.; Tubbal, F.; Raad, R. E-shaped H-slotted dual band mmWave antenna for 5G technology. *Electronics* **2021**, *10*, 1019. [CrossRef]
11. Akbari, M.; Ghalyon, H.A.; Farahani, M.; Sebak, A.-R.; Denidni, T.A. Spatially Decoupling of CP Antennas Based on FSS for 30-GHz MIMO Systems. *IEEE Access* **2017**, *5*, 6527–6537. [CrossRef]
12. Rahman, S.; Ren, X.C.; Altaf, A.; Irfan, M.; Abdullah, M.; Muhammad, F.; AlKahtani, F.S. Nature inspired MIMO antenna system for future mmWave technologies. *Micromachines* **2020**, *11*, 1083. [CrossRef] [PubMed]
13. Al Abbas, E.; Ikram, M.; Mobashsher, A.T.; Abbosh, A. MIMO Antenna System for Multi-Band Millimeter-Wave 5G and Wideband 4G Mobile Communications. *IEEE Access* **2019**, *7*, 181916–181923. [CrossRef]
14. Sharma, A.; Sarkar, A.; Adhikary, M.; Biswas A.; Akhtar, M.J. SIW fed MIMO DRA for future 5G applications. In Proceedings of the 2017 IEEE International Symposium on Antennas and Propagation & USNC/URSI National Radio Science Meeting, San Diego, CA, USA, 9–14 July 2017; pp. 1763–1764. [CrossRef]
15. KIbrahim, A.A.; Ali, W.A.E.; Alathbah, M.; Sabek, A.R. Four-Port 38 GHz MIMO Antenna with High Gain and Isolation for 5G Wireless Networks. *Sensors* **2023**, *23*, 3557. [CrossRef] [PubMed]
16. Iqbal, A.; A Saraereh, O.; Bouazizi, A.; Basir, A. Metamaterial-based highly isolated MIMO antenna for portable wireless applications. *Electronics* **2018**, *7*, 267. [CrossRef]
17. Costanzo, S.; Venneri, F.; Borgia, A.; Di Massa, G. Dual-band dual-linear polarization reflectarray for mmWaves/5G application. *IEEE Access* **2020**, *8*, 78183–78192. [CrossRef]
18. Buonanno, G.; Solimene, R. Comparing different schemes for random array. *Prog. Electromagn. Res.* **2016**, *71*, 107–118. [CrossRef]
19. Wang, Y.; Du, Z. A wideband printed dual-antenna with three neutralization lines for mobile terminals. *IEEE Trans. Antennas Propag.* **2014**, *62*, 1495–1500. [CrossRef]

20. Xing, H.; Wang, X.; Gao, Z.; An, X.; Zheng, H.-X.; Wang, M.; Li, E. Efficient Isolation of an MIMO Antenna Using Defected Ground Structure. *Electronics* **2020**, *9*, 1265. [CrossRef]
21. Dey, S.; Dey, S.; Koul, S.K. Isolation improvement of MIMO antenna using novel EBG and hair-pin shaped DGS at 5G millimeter wave band. *IEEE Access* **2021**, *9*, 162820–162834. [CrossRef]
22. Malathi, A.C.J.; Thiripurasundari, D. Review on isolation techniques in MIMO antenna systems. *Indian J. Sci. Technol.* **2016**, *9*, 1–10.
23. Nadeem, I.; Choi, D.-Y. Study on mutual coupling reduction technique for MIMO antennas. *IEEE Access* **2018**, *7*, 563–586. [CrossRef]
24. Alibakhshikenari, M.; Babaeian, F.; Virdee, B.S.; Aïssa, S.; Azpilicueta, L.; See, C.H.; Limiti, E. A comprehensive survey on "Various decoupling mechanisms with focus on metamaterial and metasurface principles applicable to SAR and MIMO antenna systems". *IEEE Access* **2020**, *8*, 192965–193004. [CrossRef]
25. Zhang, S.; Ying, Z.; Xiong, J.; He, S. Ultrawideband MIMO/diversity antennas with a tree-like structure to enhance wideband isolation. *IEEE Antennas Wirel. Propag. Lett.* **2009**, *8*, 1279–1282. [CrossRef]
26. Cuneray, K.; Akcam, N.; Okan, T.; Arican, G.O. 28/38 GHz dual-band MIMO antenna with wideband and high gain properties for 5G applications. *AEU Int. J. Electron. Commun.* **2023**, *162*, 154553. [CrossRef]
27. Kuzu, S.; Akcam, N. Array antenna using defected ground structure shaped with fractal form generated by Apollonius circle. *IEEE Antennas Wirel. Propag. Lett.* **2016**, *16*, 1020–1023. [CrossRef]
28. Govindan, T.; Palaniswamy, S.K.; Kanagasabai, M.; Kumar, S.; Marey, M.; Mostafa, H. Design and analysis of a flexible smart apparel MIMO antenna for bio-healthcare applications. *Micromachines* **2022**, *13*, 1919. [CrossRef]
29. Ravi , K.C.; Kumar, J. Miniaturized Parasitic Loaded High-Isolation MIMO Antenna for 5G Applications. *Sensors* **2022**, *22*, 7283. [CrossRef]
30. Abbas, M.A.; Allam, A.; Gaafar, A.; Elhennawy, H.M.; Sree, M.F.A. Compact UWB MIMO Antenna for 5G Millimeter-Wave Applications. *Sensors* **2023**, *23*, 2702. [CrossRef]